Reversal of Reactivity in Diene-Complexed *o*-Quinone Methide Complexes: Insights and Explanations from ab Initio Density Functional Theory Calculations

Daniel A. Lev and Douglas B. Grotjahn*

Department of Chemistry, San Diego State University, 5500 Campanile Drive, San Diego, California 92182-1030

Hani Amouri*

Laboratoire de Chimie Inorganique et Matériaux Moléculaires UMR CNRS 7071, Université Pierre et Marie Curie, 4 place Jussieu, case 42, 75252 Paris Cedex 05, France

Received May 24, 2005

The simplest *o*-quinone methide (*o*-QM, 2-methylenecyclohexa-3,5-dienone) has only been detected spectroscopically at temperatures below −100 °C, yet its derivatives have been implicated as highly reactive intermediates in organic reactions, including cycloaddition chemistry and DNA modification because of the high electrophilicity of the exocylic methylene carbon. In striking contrast, *o*-QM complexes of Cp*Ir and Cp*Rh can be isolated, characterized by X-ray diffraction, and show *nucleophilic* reactivity at the exocyclic carbon. To explain the differences in structure and reactivity as a function of metal fragment and ligand substitution pattern, we report a series of DFT calculations on Ir, Rh, and heretofore intractable Co congeners, along with a representative (arene)Ru analogue. At the B3LYP level with a variety of basis sets, the bend of the *o*-QM ligand is predicted to increase from Co to Rh to Ir, confirming solid-state data on complexes from the second- and third-row metals. In addition, an attentuation of nucleophilicity is predicted as substitution of the exocyclic methylene carbon is increased. These calculations are the first on *o*-QM complexes and are expected to guide further synthetic and reactivity studies.

Introduction

The *o*-quinone methides (*o*-QM) are highly reactive species that have been implicated as intermediates in a number of biological systems and organic reactions. The *o*-QM system is an α,β-unsaturated ketone (Figure 1) and reacts as a 1,4-Michael acceptor with nucleophiles and a Diels−Alder diene with even weak dienophiles. Reactions of *o*-QM derivatives are exceptionally facile compared with those of traditional Michael acceptors and dienes because aromatization energy provides additional product and transition state stabilization in the case of the *o*-QM fragment.[1]

As a result of high reactivity, observation of the parent *o*-QM itself has only been accomplished in an argon matrix at 10 K.[2] Despite this, *o*-QMs are readily generated as reactive intermediates which are trapped by nucleophiles or dienophiles, by methods including dehydration of *o*-hydroxybenzyl alcohols by pyrolysis,[3] photolysis,[4] and Lewis acid catalysis.[5] Additionally,

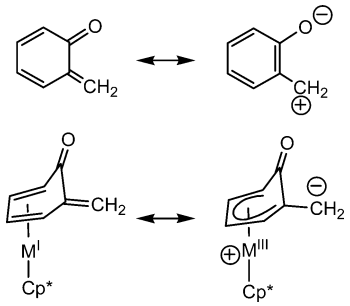

Figure 1. Resonance forms of (a) free *o*-quinone methide (*o*-QM) and (b) diene-complexed *o*-QM (M = Rh or Ir).

deamination,[6] [1,5]-sigmatropic rearrangement,[7] oxidation,[8] and cheleotropic rearrangement[9] have been used to generate *o*-QM species. This reactivity has been exploited in a number of biomimetic syntheses.[10]

* Authors for correspondence. (D.B.G.) E-mail: grotjahn@chemistry.sdsu.edu.

(1) Wan, P.; Barker, B.; Diao, L.; Fischer, M.; Shi, Y.; Yang, C. *Can. J. Chem.* **1996**, *74*, 465−475.

(2) (a) Tomioka, H. *Pure Appl. Chem.* **1997**, *69*, 837−840. (b) Tomioka, H.; Matsushita, T. *Chem. Lett.* **1997**, *26*, 399−400. (c) Qiao, G. G.; Lenghaus, K.; Solomon, D. H.; Reisinger, A.; Bytheway, I.; Wentrup, C. *J. Org. Chem.* **1998**, *63*, 9806−9811.

(3) Paul, G. C.; Gajewski, J. J. *J. Org. Chem.* **1993**, *58*, 5060−5062.

(4) Diao, L.; Yang, C.; Wan, P. *J. Am. Chem. Soc.* **1995**, *117*, 5369−5370.

(5) Chiba, K.; Hirano, T.; Kitano, Y.; Tada, M. *Chem. Commun.* **1999**, 691−692.

(6) Chiang, Y.; Kresge, A. J.; Zhu, Y. *J. Am. Chem. Soc.* **2001**, *123*, 8089−8094.

(7) Leo, E. A.; Delgado, J.; Domingo, L. R.; Espinos, A.; Miranda, M. A.; Tormos, R. *J. Org. Chem* **2003**, *68*, 9643−9647.

(8) Chiba, K.; Yamaguchi, Y.; Tada, M. *Tetrahedron Lett.* **1998**, *39*, 9035−9038.

(9) Lau, C. K.; Mintz, M.; Bernstein, M. A.; Dufresne, C. *Tetrahedron Lett.* **1995**, *34*, 5527−5530.

(10) (a) Water, R. W. V. D.; Pettus, T. R. R. *Tetrahedron* **2002**, *58*, 5367−5405. (b) Crawley, S. L.; Funk, R. L. *Org. Lett.* **2003**, *5*, 3169−3171. (c) Adlington, R. M.; Baldwin, J. E.; Mayweg, A. V. W.; Pritchard, G. J. *Org. Lett.* **2002**, *4*, 3009−3011.

10.1021/om0504093 CCC: $30.25
Publication on Web 07/21/2005

Of particular interest are small molecules that purportedly generate an *o*-QM species in a reaction with a biological molecule. Such small molecules include antibiotics,[11] vitamins,[12] and chemotherapy drugs.[13] Of primary interest is the mechanism by which *o*-QM intermediates alkylate DNA, which is responsible for their high cytotoxicity.[14]

The stabilization of *o*-QMs, and QMs in general, by transition metals is a more recent topic of interest, but already a number of groups have generated promising results. Since their 1994 report, Harman and co-workers have applied the dearomatization reagent $Os(NH_3)_5^{2+}$ to stabilize and isolate various substituted *o*-QMs, which reacted inter- and intramolecularly with electron-rich dienes to form chromans.[15] Harman's seminal work has led to the synthesis, often stereoselectively, of a number of interesting natural products.[16] In general the synthesis of these complexes involves an aldol condensation of a phenol-Os^{II} complex with an aldehyde with spontaneous dehydration of the resultant diol. In all of these cases, the stabilized QM fragment reacts like the uncomplexed organic fragment, for example as a Michael acceptor or a Diels–Alder diene.

Milstein and co-workers have elegantly synthesized *p*-quinone methide complexes of both Pd and Rh via a number of routes,[17] including a remarkable Pd^0(dtbpp) complex of the simple (i.e., unsubstituted) *p*-QM prepared by fluoride-mediated elimination reaction on a trimethylsilylated phenol complex.[17b] These complexes have been fully characterized, and their bonding has been described as the stabilization of the reactive aromatic system by stabilization of one of the C–C double bonds of the conjugated system, However, further reactions of synthetic utility have not been reported; for all intents and purposes, the benzylic carbon apparently retains its electrophilic nature,[17b] with retention of the nucleophilic or basic character of the *p*-QM oxygen.[17c]

In contrast, in 1998 Amouri and co-workers reported the synthesis and characterization of stable complexes of simple *o*-QM derivatives of the form Cp*M(*o*-QM) (M = Ir, Figure 1).[18] These complexes were obtained by double deprotonation of the *o*-alkyl phenol complexes. Not only were the complexes stable enough to be isolated and examined by X-ray diffraction, but equally remarkably, the metal-stabilized *o*-QM species showed a complete reversal of reactivity, wherein the normally electrophilic exocyclic methylene carbon had become nucleophilic upon transition metal coordination. For example, in Cp*Ir(*o*-QM) the exocyclic carbon undergoes nucleophilic substitution reactions, e.g. with iodine or methyl propiolate, and [3+2] dipolar cycloadditions, as in the case of the electron-poor dienophile *N*-methylmaleimide (Scheme 1).[19]

Scheme 1. Reversal of Reactivity in Cp*Ir Stabilized *o*-QM Complexes

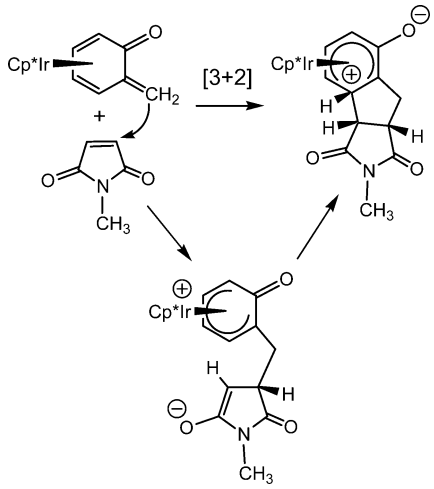

This reactivity has been explained in terms of an M^{III} resonance form in which the carbon can be viewed as bearing a negative charge (Figure 1).[19a] Additionally, it was hypothesized that the stabilization of *o*-QM species could be correlated to the degree of deviation of the carbonyl/alkene portion of the *o*-QM from planarity with the coordinated diene portion—a parameter referred to as the hinge angle—which results from metal back-bonding into the aromatic system.[19b] This observation has been previously reported for a number of analogous zerovalent Fe, Ru and Os xylylene π complexes.[20] Like the Cp*M(*o*-QM) complexes, these metal xylylene complexes react with the strong electrophiles, such as HOTf, HPF_6, and $CH_3SO_3CH_3$. However, unlike *o*-QM complexes discussed in this paper, they do not undergo Diels–Alder reactions, other cycloadditions, or conjugate additions.[20d]

In this paper we shed light on Cp*M stabilization of *o*-QMs and the remarkable reversibility observed in the reactivity of the organic fragment. To do so we have taken an ab initio computational approach, employing

(11) Tomasz, M.; Chawla, A. K.; Lipman, R. *Biochemistry* **1988**, *27*, 3182.

(12) (a) Swartz, A. M.; Barra, M.; Kuntz, D. *J. Org. Chem.* **2004**, *69*, 3198–3201. (b) Rosenau, T.; Potthast, A.; Hofinger, A.; Kosma, P. *Angew. Chem., Int. Ed.* **2002**, *41*, 1171–1173.

(13) (a) Angle, S. R.; Rainier, J. D.; Woytowicz, C. *J. Org. Chem.* **1997**, *62*, 5884–5892. (b) Rietjens, I. M. C. M.; Awad, H. M.; Boersma, M. G.; van Iersel, M. L. P. S.; Vervoort, J.; Van Bladeren, P. J. *Adv. Exp. Med. Biol*. **2001**, *500*, 11–21. (c) Awad, H. M.; Boersma, M. G.; Boeren, S.; van Bladeren, P. J.; Vervoort, J.; Rietjens, I. M. C. M. *Chem. Res. Toxicol.* **2001**, *14*, 398–408.

(14) (a) Zhou, Q.; Turnbull, K. D. *J. Org. Chem.* **1999**, *64*, 2847–2851. (b) Pande, P.; Shearer, J.; Yang, J.; Greenberg, W. A.; Rokita, S. E. *J. Am. Chem. Soc.* **1999**, *121*, 6774–6779. (c) Freccero, M.; Gandolfi, R.; Sarzi-Amade, M. *J. Org. Chem.* **2003**, *68*, 6411–6423. (d) Di Valentin, C.; Freccero, M.; Zanaletti, R.; Sarzi-Amade, M. *J. Am. Chem. Soc.* **2001**, *123*, 8366–8377. (e) Veldhuyzen, W. F.; Shallop, A. J.; Jones, R. A.; Rokita, S. E. *J. Am. Chem. Soc.* **2001**, *123*, 11126–11132. (f) Freccero, M.; Di Valentin, C.; Sarzi-Amade, M. *J. Am. Chem. Soc.* **2003**, *125*, 3544–3553. (g) Modica, E.; Zanaletti, R.; Freccero, M.; Mella, M. *J. Org. Chem.* **2001**, *66*, 41–52.

(15) (a) Kopach, M. E.; Harman, W. D. *J. Am. Chem. Soc.* **1994**, *116*, 6581–6592. (b) Stokes, S. M., Jr.; Ding, F.; Smith, P. L.; Keane, J. M.; Kopach, M. E.; Jervis, R.; Sabat, M.; Harman, W. D. *Organometallics* **2003**, *22*, 4170–4171.

(16) Harman, W. D. *Chem. Rev.* **1997**, *97*, 1953–1978.

(17) (a) Vigalok, A.; Milstein, D. *J. Am. Chem. Soc.* **1997**, *119*, 7873–7874. (b) Rabin, O.; Vigalok, A.; Milstein, D. *J. Am. Chem. Soc.* **1998**, *120*, 7119–7120. (c) Vigalok, A.; Shimon, L. J. W.; Milstein, D. *J. Am. Chem. Soc.* **1998**, *120*, 477–483.

(18) Amouri, H.; Besace, Y.; Bras, J. L.; Vaissermann, J. *J. Am. Chem. Soc.* **1998**, *120*, 6171–6172.

(19) (a) Amouri, H.; Vaissermann, J.; Rager, M. N.; Grotjahn, D. B. *Organometallics* **2000**, *19*, 1740–1748. (b) Amouri, H.; Bras, J. L. *Acc. Chem. Res.* **2002**, *35*, 501–510.

(20) (a) Bennett, M. A. *Coord. Chem. Rev.* **1997**, *166*, 225–254. (b) Hull, J. W.; Gladfelter, W. L. *Organometallics* **1982**, *1*, 1716–1718. (c) Bennett, M. A.; Goh, L. Y.; McMahon, I. J.; Mitchell, T. R. B.; Robertson, G. B.; Turney, T. W.; Wasantha, W. *Organometallics* **1992**, *11*, 3069–3085. (d) Hull, J. W.; Mann, C.; Gladfelter, W. L. *Organometallics* **1992**, *11*, 3117–3121. (e) Bennett, M. A.; Bown, M.; Goh, L. Y.; Hockless, D. C. R.; Mitchell, T. R. B. *Organometallics* **1995**, *14*, 1000–1007. (f) Madonik, A. M.; Astruc, D. *J. Am. Chem. Soc.* **1984**, *106*, 2437–2439.

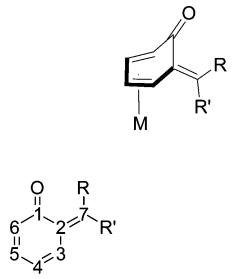

IrMe$_2$: M = Cp*Ir; R = Me; R' = Me
RhMe$_2$: M = Cp*Rh; R = Me; R' = Me
IrH$_2$: M = Cp*Ir; R = H; R' = H
RhH$_2$: M = Cp*Rh; R = H; R' = H
CoH$_2$: M = Cp*Co; R = H; R' = H
RuH$_2$: M = C_6Me_6Ru; R = H; R' = H
RhMe$_{cis}$: M = Cp*Rh; R = Me; R' = H
RhMe$_{trans}$: M = Cp*Rh; R = H; R' = Me
IrMe$_{cis}$: M = Cp*Ir; R = Me; R' = H
IrMe$_{trans}$: M = Cp*Ir; R = H; R' = Me
RhPh$_2$: M = Cp*Rh; R = Ph; R' = Ph

Figure 2. Structures considered in the computational analysis.

the hybrid density functional B3LYP method. We have examined the gas phase structure, bonding, and charge density of the series of complexes shown in Figure 2 and compared the results with previously published solid-state structures of Cp*M(*o*-QM). A similar method was used to examine the bonding and structure of octahedral Ru^{II} xylylene complexes, but the focus of this previous study was the overall structure of the class of compounds rather than explaining their reactivity,[21] both of which are considered in the present paper.

In comparison, the potent reactivity of uncomplexed *o*-QMs with DNA and other small biological moleules has been studied at the B3LYP level.[7,14c,d,f,g] In particular, nucleophilic additions by the free bases of DNA were studied with an emphasis on the function of water in the tightly hydrogen-bonded transition states. These studies have invariably shown that the quinone methide is a highly polarized molecule that forms strong inter- and intramolecular hydrogen bonds, which are critical to nucleophilic approach and rearrangement pathways.[14f] The electrophilicity of the quinone methide was correlated to the partial charge (CHelpG) on the *o*-QM oxygen atom and the overall molecular dipole.[14c]

Experimental Section

Selection of Computational Methods. The B3LYP method is now widely used in the description of transition metal organometallic complexes.[22] It has been compared to various high-level computational methods and been found to be an excellent compromise between efficiency and accuracy.[23] Effective core potentials have also been demonstrated to effectively account for relativistic effects in transition metal bonding. By employing B3LYP hybrid density functional methods with a Los Alamos National Labs effective core potential (LANL2) many systems have been studied with sufficient accuracy to reproduce experimental results.[24] The choice of a second basis set for treatment of the main group ligand atoms and metal valence electrons is crucial to obtaining reliable energies. However, very large basis set models present a problem from the view of computational efficiency. To this end optimizations at the relatively equivalent valence double-ζ or split valence 6-31G level followed by single-point energy calculations at the triple-ζ or 6-311G level have proven effective. Additionally, polarization functions are crucial to accurately depict the bonding in transition metal complexes, especially for the atoms directly bonded to metal center. However, addition of polarization functions to the metal itself is generally not necessary, as *f* functions are not apparently involved in the bonding in any significant way.

Implementation. All calculations were carried out using the Gaussian 98[25] and Gaussian 03[26] program packages. All structures were first computed at the B3LYP[27] level using the LANL2DZ basis set as it is implemented in the Gaussian programs. This basis set uses the effective core potential of Hay and Wadt[28] to describe the core electrons of the metal atom, Co (341/311/41), Ru (341/321/31), Rh (341/321/31), and Ir (341/321/21). The valence electrons of the metal atom in addition to those of H, C, and O are treated by the Dunning−Huzinaga double-ζ basis set (D95).[29] These basis sets were augmented by the addition of a single polarization function to all H, C, and O atoms, designated in the text as LANL2DZ**. In some cases a single *f* polarization function was also added to the metal atom.[30] In addition the SDD basis set as it is implemented in the Gaussian programs was employed for purposes of effective core potential comparison. This basis set uses the Stuttgart−Dresden effective core potential of Dolg and co-workers[31] for the transition metals—Co (311111/22111/411/1), Ru (311111/22111/411), Rh (311111/22111/411), and Ir (311111/22111/411)—in conjunction with the same D95[29] basis set. When polarization functions have been added to the descriptions of H, C, and O atoms in this basis set, it is designated SDD** in the text. We have also performed comparisons with the higher-level and split valence basis sets in which we have replaced D95 by the 6-31G,[32] TZV,[33] and 6-311G[34] basis sets for all H, C, N, and O atoms, leaving the LANL2DZ basis set on the transition metal intact.

(21) McGrady, J. E.; Stranger, R.; Bown, M.; Bennett, M. A. *Organometallics* **1996**, *15*, 3109−3114.
(22) (a) Lupinetti, A. J.; Jonas, V.; Thiel, W.; Strauss, S. H.; Frenking, G. *Chem. Eur. J.* **1999**, *5*, 2563−2583. (b) Dedieu, A. *Top. Organometallic Chem.* **1999**, *4*, 69−107.
(23) Berezin, K. V.; Nechaev, V. V. *J. Appl. Spectrosc.* **2004**, *71*, 164−172.
(24) Mainz, D. T.; Klicic, J. J.; Friesner, R. A.; Langlois, J.-M.; Perry, J. K. *J. Comput. Chem.* **1997**, *17*, 1863−1874.
(25) Frisch, M. J.; Trucks, G. W.; Schlegel, H. B.; Scuseria, G. E.; Robb, M. A.; Cheeseman, J. R.; Zakrzewski, V. G.; Montgomery, J. A.; Stratmann, R. E.; Burant, J. C.; Dapprich, S.; Millam, J. M.; Daniels, A. D.; Kudin, K. N.; Strain, M. C.; Farkas, O.; Tomasi, J.; Barone, V.; Cossi, M.; Cammi, R.; Mennucci, B.; Pomelli, C.; Adamo, C.; Clifford, S.; Ochterski, J.; Petersson, G. A.; Ayala, P. Y.; Cui, Q.; Morokuma, K.; Malick, D. K.; Rabuck, A. D.; Raghavachari, K.; Foresman, J. B.; Cioslowski, J.; Ortiz, J. V.; Stefanov, B. B.; Liu, G.; Liashenko, A.; Piskorz, P.; Komaromi, I.; Gomperts, R.; Martin, R. L.; Fox, D. J.; Keith, T.; Al-Laham, M. A.; Peng, C. Y.; Nanayakkara, A.; Gonzalez, C.; Challacombe, M.; Gill, P. M. W.; Johnson, B. G.; Chen, W.; Wong, M. W.; Andres, J. L.; Head-Gordon, M.; Replogle, E. S.; Pople, J. A. *Gaussian 98*; Gaussian, Inc.: Pittsburgh, PA, 1998.
(26) Frisch, M. J.; Trucks, G. W.; Schlegel, H. B.; Scuseria, G. E.; Robb, M. A.; Cheeseman, J. R.; Montgomery, J. A., Jr.; Vreven, T.; Kudin, K. N.; Burant, J. C.; Millam, J. M.; Iyengar, S. S.; Tomasi, J.; Barone, V.; Mennucci, B.; Cossi, M.; Scalmani, G.; Rega, N.; Petersson, G. A.; Nakatsuji, H.; Hada, M.; Ehara, M.; Toyota, K.; Fukuda, R.; Hasegawa, J.; Ishida, M.; Nakajima, T.; Honda, Y.; Kitao, O.; Nakai, H.; Klene, M.; Li, X.; Knox, J. E.; Hratchian, H. P.; Cross, J. B.; Adamo, C.; Jaramillo, J.; Gomperts, R.; Stratmann, R. E.; Yazyev, O.; Austin, A. J.; Cammi, R.; Pomelli, C.; Ochterski, J. W.; Ayala, P. Y.; Morokuma, K.; Voth, G. A.; Salvador, P.; Dannenberg, J. J.; Zakrzewski, V. G.; Dapprich, S.; Daniels, A. D.; Strain, M. C.; Farkas, O.; Malick, D. K.; Rabuck, A. D.; Raghavachari, K.; Foresman, J. B.; Ortiz, J. V.; Cui, Q.; Baboul, A. G.; Clifford, S.; Cioslowski, J.; Stefanov, B. B.; Liu, G.; Liashenko, A.; Piskorz, P.; Komaromi, I.; Martin, R. L.; Fox, D. J.; Keith, T.; Al-Laham, M. A.; Peng, C. Y.; Nanayakkara, A.; Challacombe, M.; Gill, P. M. W.; Johnson, B.; Chen, W.; Wong, M. W.; Gonzalez, C.; Pople, J. A. *Gaussian 03*, Revision B.02; Gaussian, Inc.: Pittsburgh, PA, 2003.
(27) (a) Becke, A. D. *J. Chem. Phys.* **1993**, *98*, 5648. (b) Lee, C.; Yang, W.; Parr, R. G. *Phys. Rev. B* **1988**, *37*, 785−789.
(28) Hay, P. J.; Wadt, W. R. *J. Chem. Phys.* **1985**, *82*, 270−283.
(29) Dunning, T. H., Jr.; Hay, P. J. In *Modern Theoretical Chemistry*; Schaefer, H. F., III, Ed.; Plenum: New York, 1976; Vol. 3, p 1.
(30) Ehlers, A. W.; Boehme, M.; Dapprich, S.; Gobbi, A.; Hoellwarth, A.; Jonas, V.; Koehler, K. F.; Stegmann, R.; Veldkamp, A.; et al. *Chem. Phys. Lett.* **1993**, *208*, 111−114.
(31) Wedig, U.; Dolg, M.; Stoll, H.; Preuss, H. In *Quantum Chemistry: The Challenge of Transition Metals and Coordination Chemistry*; Veillard, A., Ed.; Reidel: Dordrecht, The Netherlands, 1986; p 79.
(32) (a) Ditchfield, R.; Hehre, W. J.; Pople, J. A. *J. Chem. Phys.* **1971**, *54*, 724. (b) Hehre, W. J.; Ditchfield, R.; Pople, J. A. *J. Chem. Phys.* **1972**, *56*, 2257. (c) Hariharan, P. C.; Pople, J. A. *Theor. Chim. Acta* **1973**, *28*, 213. (d) Hariharan, P. C.; Pople, J. A. *Mol. Phys.* **1974**, *27*, 209.
(33) Schaefer, A.; Huber, C.; Ahlrichs, R. *J. Chem. Phys.* **1994**, *100*, 5829.

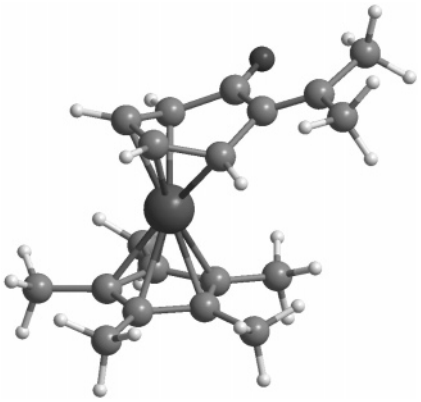

Figure 3. B3LYP/LANL2DZ** optimized structure of **IrMe**$_2$.

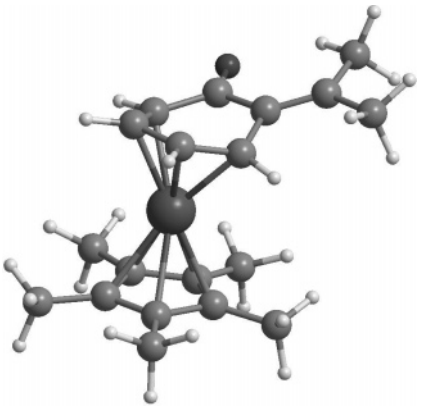

Figure 4. B3LYP/LANL2DZ** optimized structure of **RhMe**$_2$.

All structures were fully optimized as stationary points on the potential energy surface and verified by frequency analysis (NIMAG = 0), from which zero-point energies were also obtained. Population analyses based on the SCF densities were performed using the standard methods of the Gaussian programs, e.g. Mulliken, natural bond order,[35] and atomic polarizability tensors.

Results and Discussion

Comparison of Calculated Structures to Existing X-ray Diffraction Data. Comparison of the structures of *o*-QM species computed at the B3LYP/LANL2DZ** level to the known solid-state geometries reveals close agreement between experiment and calculation. X-ray diffraction structures have been solved for only two compounds: one is a close analogue of dimethyl-substituted species **IrMe**$_2$ but differing slightly in that an isopropyl substituent is present at the terminal diene carbon C^6.[18] The other is the dimethyl-substituted species corresponding to **RhMe**$_2$.[36] Therefore, we have compared the computed structures of **IrMe**$_2$ and **RhMe**$_2$ (Figures 3 and 4, respectively) to the XRD structures which have been previously reported (Table 1).

As seen in Table 1, in the case of **IrMe**$_2$, the Ir−C distances of the Cp* fragment followed the same general trend as the solid-state structure,[18] in which the Cp* ring is tilted away from the π-bound diene portion of the *o*-QM ligand. In contrast to the solid-state structure, a single carbon of the Cp ring has a shorter Ir−C distance, with the other four carbons relatively symmetrically bound to the Ir. In the solid state, a single carbon disposed across from the diene fragment has a longer Ir−C distance, with the other four carbons relatively symmetrically bound. Neglecting this structural difference, deviations from the XRD structure are in the range of 0.05−0.11 Å. The largest deviation in Ir−C distance is seen for the carbon atoms trans to the internal carbons (C^4 and C^5) of the diene subunit, and the smallest, for the carbon atoms trans to the outer carbons (C^3 and C^6) of the diene subunit. In **IrMe**$_2$, the Ir−C bond distances of the diene subunit deviate from those of the XRD structure by 0.005−0.063 Å, where again the largest deviations are seen for the C^4 and C^5 of the diene subunit. Bond distances in **IrMe**$_2$ are more symmetrical than in the XRD structure, but this likely results from the additional isopropyl substitution at C^6 in the experimental complex. In the solid-state structure, the terminal diene carbon C^6 with an isopropyl substituent is further from the Ir center by 0.024 Å, than is the other terminal diene carbon C^3, which bears only a hydrogen. This can be rationalized in terms of the steric interaction between the isopropyl group and the Cp*Ir fragment. To maintain planarity of the diene subunit, the internal diene carbon C^5 adjacent to isopropyl-substituted C^6 is also further, 0.021 Å, from the Ir atom than the other internal diene carbon C.[4] Substitution in the experimental structure precludes direct comparison of the effects of asymmetry on the bonding of the *o*-QM fragment, which appear to be negligible in **IrMe**$_2$, where Ir−C^6 = 2.198 Å and Ir−C^3 = 2.206 Å. Bond distances and angles within the *o*-QM portion of **IrMe**$_2$ are nearly within the standard deviations of the XRD structure, with the only notable exceptions of ∼0.03 Å occurring in the C^3−C^2 and C^3−C^4 bonds adjacent to the isopropyl substituent. The hinge angle of the *o*-QM ligand in **IrMe**$_2$ is 38°, versus 33° in the XRD structure.

For complex **RhMe**$_2$ direct comparison to various computational models is possible, because the experimental XRD molecular structure has been solved.[36] Analogous to **IrMe**$_2$ the Cp* ring is tilted away from the diene subunit of the *o*-QM ligand. In contrast to **IrMe**$_2$, the Rh−C distances to the Cp* ligand are longer than the solid-state distances by ∼0.1 Å. Herein a comparison can be made between the effects of the asymmetry of the *o*-QM ligand. In the solid state, the Cp* carbons trans to the methide portion of the *o*-QM ligand are 0.10 Å closer to the Rh center. However, the computed structure did not reproduce this result. Switching to a Stuttgart−Dresden effective core potential shortened the Rh−C bonds in **RhMe**$_2$ by 0.02−0.04 Å but did not reproduce the bonding asymmetry of the solid-state structure. Comparison of Rh−C bond lengths in the diene subunit of **RhMe**$_2$ to those in the XRD structure reveals close semblance, with the LANL2DZ** distances 0.06−0.07 Å longer than the experimental results and the SDD** distances 0.04−0.05 Å longer. The SDD**

(34) Krishnan, R.; Binkley, J. S.; Seeger, R.; Pople, J. A. *J. Chem. Phys.* **1980**, *72*, 650.
(35) (a) Carpenter, J. E.; Weinhold, F. *J. Mol. Struct. (THEOCHEM)* **1988**, *169*, 41. (b) Reed, A. E.; Curtiss, L. A.; Weinhold, F. *Chem. Rev.* **1988**, *88*, 899−926.
(36) Amouri, H.; Vaissermann, J.; Rager, M. N.; Grotjahn, D. B. *Organometallics* **2000**, *19*, 5143−5148.

Table 1. Comparison of Bond Lengths (Å) and Angles (deg) of Computed *o*-QM Metal Complexes with XRD Solid-State Structures

	$IrMe_2$			$RhMe_2$		
	LANL2[a]	SD[a]	XRD[b]	LANL2[a]	SD[a]	XRD[c]
$M-C^3$	2.206	2.207	2.169(8)	2.248	2.230	2.189(7), 2.163(7)
$M-C^4$	2.185	2.177	2.122(9)	2.181	2.166	2.112(8), 2.143(7)
$M-C^5$	2.185	2.177	2.143(9)	2.178	2.163	2.115(8), 2.141(7)
$M-C^6$	2.198	2.199	2.193(8)	2.232	2.213	2.178(8), 2.189(7)
$M-Cp^1$	2.245	2.246	2.180(8)	2.269	2.251	2.183(7), 2.180(7)
$M-Cp^2$	2.269	2.266	2.179(8)	2.265	2.250	2.163(8), 2.168(7)
$M-Cp^3$	2.365	2.358	2.220(7)	2.373	2.343	2.143(7), 2.182(7)
$M-Cp^4$	2.345	2.338	2.246(7)	2.346	2.314	2.262(7), 2.248(7)
$M-Cp^5$	2.259	2.257	2.208(7)	2.271	2.254	2.244(7), 2.289(7)
C^1-C^2	1.499	1.499	1.49(1)	1.503	1.501	1.48(1), 1.48(1)
C^2-C^3	1.495	1.495	1.46(1)	1.487	1.488	1.48(1), 1.48(1)
C^3-C^4	1.460	1.458	1.42(1)	1.438	1.440	1.42(1), 1.43(1)
C^4-C^5	1.437	1.437	1.43(1)	1.434	1.434	1.41(1), 1.39(1)
C^5-C^6	1.461	1.459	1.44(1)	1.440	1.443	1.40(1), 1.43(1)
C^6-C^1	1.490	1.489	1.48(1)	1.482	1.481	1.45(1), 1.45(1)
C^2-C^7	1.365	1.365	1.34(1)	1.367	1.367	1.35(1), 1.36(1)
C^7-O	1.249	1.250	1.23(1)	1.252	1.253	1.23(1), 1.24(1)
$C^1-C^2-C^3$	110.9	110.9	109.7(7)	112.1	111.7	112.1(7), 112.2(6)
$C^2-C^3-C^4$	120.8	121.0	120.6(8)	122.5	122.3	
$C^5-C^6-C^1$	122.1	122.3	121.4(8)	123.7	123.6	
$C^6-C^1-C^2$	112.9	113.1	114.7(7)	114.3	114.2	115.4(8), 115.5(6)
$O-C^1-C^2$	126.5	126.4	124.3(8)	125.6	125.7	124.0(8), 126.2(8)
$O-C^1-C^6$	120.5	120.4	121.0(9)	120.0	120.0	

[a] Effective core potential combined with D95**. [b] Structure is of analogue with an additional isopropyl substituent at $C.^6$ See text and ref 32. [c] Two independent molecules in unit cell. See ref 55.

structure reproduces the experimental finding that the Rh atom is closer to C^3 than $C,^6$ but the Los Alamos effective core potential does not account for this observation. As in the case of **IrMe**$_2$, the bond lengths and angles within the *o*-QM ligand itself are excellently reproduced computationally, without any basis set dependence. The hinge angle of the *o*-QM fragment in complex **RhMe**$_2$ is 30°, versus 25° in the solid-state structure. The standard deviation in the computed bond lengths as compared to the XRD structure is 0.031 Å.

We hypothesized that the degree of stabilization can be measured by the hinge angle between the plane of the diene subunit and the plane of the carbonyl-alkene subunit of the *o*-QM ligand. In the case of Ir this angle is much larger, 8° experimentally, than in the Rh case, and a substantial increase in stability was observed. This angle is likely the result of π back-donation from the metal center to the diene subunit, which disrupts the conjugation of the π system. Therefore, the energetic barrier to rearomatization involves a reordering of the metal−ligand orbitals in addition to those of the carbon π system.

Structural Comparisons of Homologues. Although the unsubstituted *o*-QM complexes of Cp*Ir[18] and Cp*Rh[36] fragments have been characterized by ^1H, ^{13}C, and COSY NMR and IR spectroscopy and the more stable Cp*Ir compound could be isolated and reacted with electrophiles to yield nucleophilic addition products,[19] XRD data for these parent species have been unattainable. Therefore, we have computationally optimized the structures of these known Cp*Ir and Cp*Rh complexes of *o*-QM as well as those of as-yet-unmade Cp*Co and (Me_6C_6)Ru analogues to examine the effect of metal fragment on the overall stabilization and reactivity of the *o*-QM system. Discussion of the overall structures follows, including consideration of hinge angle and changes in parameters as a function of substitution on the exocyclic double bond of the *o*-QM ligand.

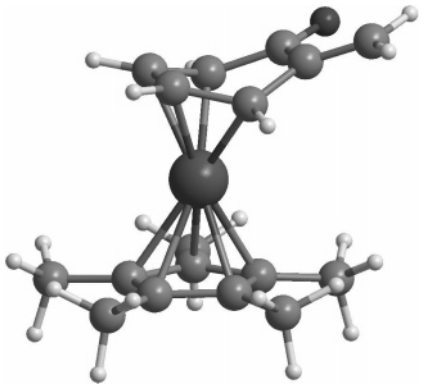

Figure 5. B3LYP/LANL2DZ** optimized structure of **IrH**$_2$.

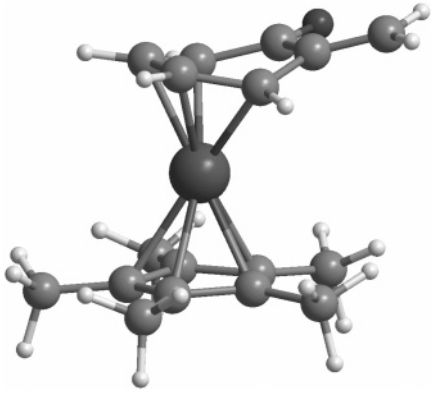

Figure 6. B3LYP/LANL2DZ** optimized structure of **RhH**$_2$.

In the simple, unsubstituted *o*-QM complexes **MH**$_2$ (Figures 5 to 8), the ancillary Cp* or arene ligand follows the same pattern of tilting away from the diene subunit of the *o*-QM ligand. This can be explained sterically by the openness of the metal coordination sphere opposite the "hinged" up portion of the *o*-QM ligand. However, a more compelling argument can be made by examining

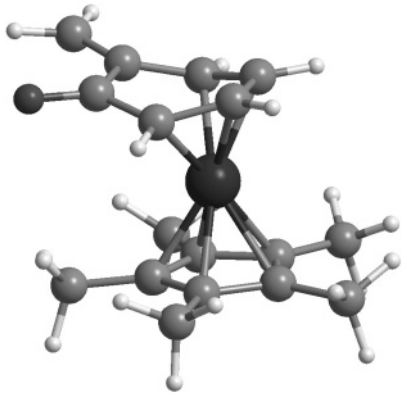

Figure 7. B3LYP/LANL2DZ** optimized structure of **CoH**$_2$.

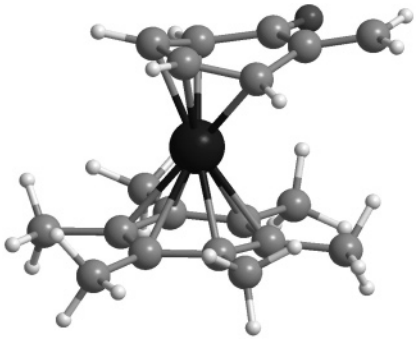

Figure 8. B3LYP/LANL2DZ** optimized structure of **RuH**$_2$.

the HOMO of the complexes. The MO bonding picture reveals strong π back-bonding between a filled metal d orbital and a π^* orbital of the *o*-QM (Figure 15), particularly the lobes localized on the diene subunit. This MO also involves a π-bonding interaction between the same metal d orbital and a filled Cp* π orbital. Since the metal−ligand d−π^* interaction is strongest with the internal diene carbons (C^4 and C^5), the strongest compensating trans influence is seen for the Cp* carbon diametrically opposed to these carbons.

Complexes **CoH**$_2$, **RhH**$_2$, **IrH**$_2$, and **RuH**$_2$ (Figures 5 to 8) exhibit a similar preference seen in complex **RhMe**$_2$ in which the metal is closer to the diene carbons adjacent to the carbonyl group (C^5 and C^6) than those adjacent to the methide group (C^3 and C^4). This trend becomes less predominant as one descends the periodic table, wherein it goes from 0.02 to 0.01 to 0.004 Å down the group 9 metals. As expected from the comparison of complexes **IrMe**$_2$ and **RhMe**$_2$ and as a result of the lanthanide contraction, M−C bond lengths follow the order Co < Ir < Rh for both the diene subunit of the *o*-QM fragment and the Cp* fragment. The bonding around the *o*-QM ligand is mostly invariant when the metal center is changed, with only a slight lengthening of the bonds in the diene subunit that follows the degree of π back-donation upon changing from Co to Rh to Ir. However, the hinge angle (Table 3) varies rather dramatically as a function of the metal fragment, where it is 25° for **CoH**$_2$, 27° for **RhH**$_2$, 36° for **IrH**$_2$, and 25° for **RuH**$_2$.

By comparison, the analogous $(C_6Me_6)Ru^0$ *o*-xylylene complex reported by Gladfelter has a hinge angle of 33.8°,[20b] and the $M(PMe_2Ph)_3$ [M = Ru, Os] *o*-xylylene complexess have hinge angles of 37° and 39.5°, respectively.[20e] In a DFT study of a simplified $Ru(PH_3)_3$ congener Bennett found a hinge angle of 35°.[21] The larger hinge angles for the *o*-xylylene complexes than in the *o*-QM may be attributed to decreased metal-to-ligand back-bonding and reduced electron density in the aromatic π-system.

As hypothesized in Os^{II} destabilization of aromatic systems, the back-donation from metal d orbitals to aromatic π^* orbitals is the main stabilizing interaction in these *o*-QM metal complexes.[15,16] Upon bonding to the transition metal the σ_v symmetrical structure becomes energetically favored by $d_{xz,yz}$ donation to the antibonding orbital of the *o*-QM fragment. The degree of this interaction increases as one descends the periodic table, which is manifested by an increase in the hinge angle.

The π back-donation is also seen in the bonding of the diene subunit. The geometry of the free *o*-QM was optimized at the B3LYP/6-311++G(3df,3pd) level and compared to geometries of **CoH**$_2$, **RhH**$_2$, **IrH**$_2$, and **RuH**$_2$. In the free organic *o*-QM the double bonds of the cyclohexadiene ring are significantly shorter than the single bonds. The C^5-C^6 double bond closer to the carbonyl group is slightly longer, 1.348 Å, than the one closer to the methylene functionality, 1.346 Å, because the C=O bond is more electron withdrawing. The internal C^4-C^5 single bond of the diene is 1.448 Å long, and the lengths of the other single bonds are 1.464, 1.511, and 1.452 Å. The length of the single bonds can be correlated to their degree of conjugation with the π system. However, **CoH**$_2$, **RhH**$_2$, **IrH**$_2$, and **RuH**$_2$ all contain lengthened double bonds and a shortened C^4-C^5 single bond in the diene portion of the *o*-QM. The bond lengths are nearly equal in the diene subunit of these complexes, wherein the formally "double" bonds (C^3-C^4 and C^5-C^6) are longer than the internal single bond (C^4-C^5) for the second- and third-row metals. Additionally, the single bonds (C^3-C^2 and C^6-C^1) adjacent to the diene are lengthened by about 0.01−0.03 Å, **IrH**$_2$ > **RhH**$_2$ > **CoH**$_2$. Both of these results corroborate with population of the *o*-QM π^* orbital. In contrast, the bonding of the α,β-unsaturated carbonyl subunit is nearly unaffected by the metal and is independent of metal fragment.

The uncoordinated exo diene moiety in the Gladfelter complex is also relatively unperturbed by complexation to Ru.[20b] The bond lengths of the symmetric complex are lengthened by 0.01 Å relative to the calculated free organic species,[37] although this may be due to the steric effect of the methyl groups present in the experimental compound. The endocylic diene is significantly affected by complexation, with a shortened internal "single" bond (by 0.03 Å) and lengthened "double" bonds (by 0.07 Å). A similar phenomenon was observed in the trisphosphine complexes of Bennett, who observed that the data supports describing the molecule as closer to an enediyl form.[21]

In addition to examining the role of the metal on *o*-QM bonding, we have also examined the effects of varying the substitution pattern on *o*-QM stability and reactivity. Complexes **IrMe**$_2$, **RhMe**$_2$, **RhMe**$_{cis}$, **RhMe**$_{trans}$, **IrMe**$_{cis}$, **IrMe**$_{trans}$, and **RhPh**$_2$ (Figures 3,

(37) Sakai, S. *J. Phys. Chem. A* **2000**, *104*, 11615−11621.

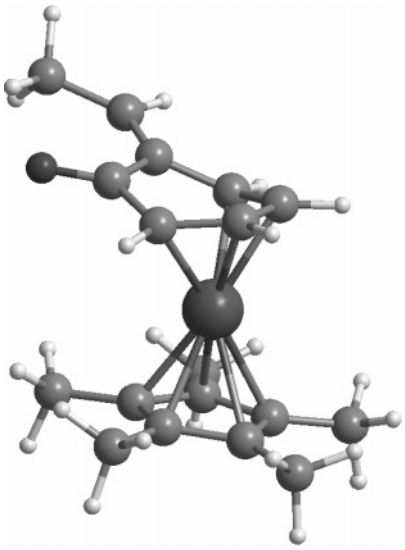

Figure 9. B3LYP/LANL2DZ** optimized structure of **RhMe**$_{cis}$.

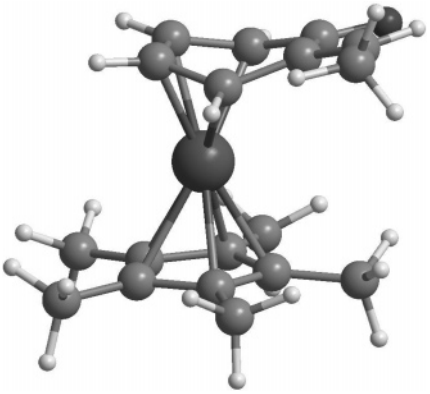

Figure 10. B3LYP/LANL2DZ** optimized structure of **RhMe**$_{trans}$.

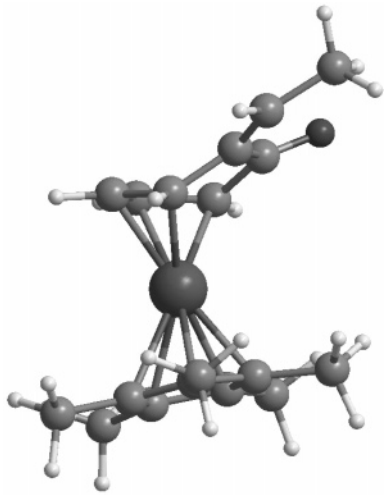

Figure 11. B3LYP/LANL2DZ** optimized structure of **IrMe**$_{cis}$.

4, and 9−14) involve varying substitution patterns of the methylene position of *o*-QM. The effects of replacing hydrogens by methyl groups were relatively minor. However, a slight effect of *E* vs *Z* monosubstitution is observed. The C^2-C^7 and C^7-C^{Me} bond lengths are invariant with respect to substitution, but a

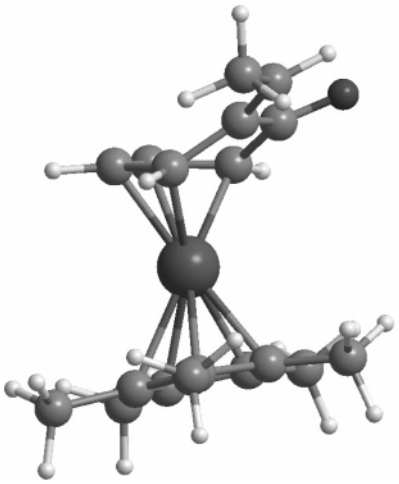

Figure 12. B3LYP/LANL2DZ** optimized structures of **IrMe**$_{trans}$.

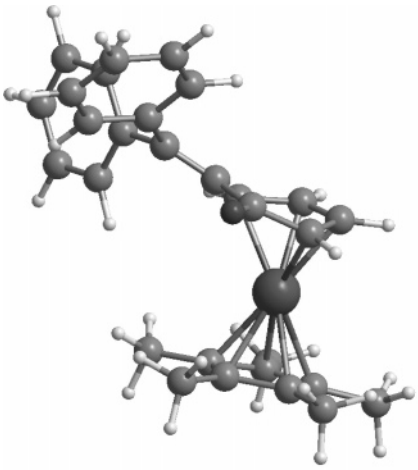

Figure 13. B3LYP/LANL2DZ** optimized structure of **RhPh**$_2$.

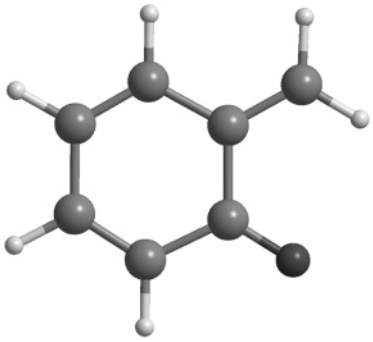

Figure 14. B3LYP/6-311++G(3df,3pd) optimized structure of ***o*-QM**.

$C^2{=}C^7{-}C^{Me}$ angle for **RhMe**$_{cis}$ that is 0.9° larger than **RhMe**$_{trans}$ indicates a steric interaction between the CH_3 group and the carbonyl oxygen. Similarly, the $C^1-C^2{=}C^7$ angle of the *Z* isomer is larger by 6.0°, with a concomitant 5.3° larger $C^7{=}C^2-C^3$ angle. The $O{=}C^1-C^2$ and $O{=}C^1-C^6$ angles of the *Z* isomer are changed by 1.1° and −1.0°, respectively, relative to the *E* isomer. Energetically, **RhMe**$_{trans}$ is only 1.1 kcal/mol more stable than **RhMe**$_{cis}$. Similarly, for the Ir congeners, **IrMe**$_{trans}$ is 0.9 kcal/mol more stable than **IrMe**$_{cis}$, and the general geometric trends are followed. In **RhPh**$_2$ the steric effect of the larger Ph substituents result in elongation of the

Table 2. Partial Charges on Relevant Atoms of *o*-QM Metal Complexes

entry	cmpd	method	basis set[a]	C^7	C^2	C^1	O	M
1	$IrMe_2$	Mulliken	LANL2	0.1623	0.3355	0.0443	−0.2838	−0.1839
2	$IrMe_2$	APT	LANL2	0.2323	−0.2919	0.8952	−0.7356	−0.5026
3	$IrMe_2$	NPA	LANL2	0.0913	−0.1632	0.5332	−0.6199	0.5050
4	$IrMe_2$	Mulliken	SDD	0.1340	0.3064	0.0339	−0.2808	−0.4617
5	$IrMe_2$	APT	SDD	0.2245	−0.2849	0.8894	−0.7395	0.5978
6	$IrMe_2$	NPA	SDD	0.0903	−0.1590	0.5291	−0.6154	0.4273
7	$RhMe_2$	Mulliken	LANL2	0.1466	0.3280	0.0319	−0.2897	−0.0587
8	$RhMe_2$	APT	LANL2	0.2266	−0.2920	0.8588	−0.7256	−0.3030
9	$RhMe_2$	NPA	LANL2	0.0917	−0.1680	0.5122	−0.6271	0.4154
10	$RhMe_2$	Mulliken	SDD	0.1220	0.3000	0.0247	−0.2866	−0.3223
11	$RhMe_2$	APT	SDD	0.2192	−0.2851	0.8644	−0.7291	−0.3607
12	$RhMe_2$	NPA	SDD	0.0907	−0.1634	0.5079	−0.6224	0.3131
13	CoH_2	Mulliken	LANL2	−0.6083	0.5591	−0.0196	−0.2724	−0.2893
14	CoH_2	APT	LANL2	−0.2321	−0.0010	0.7446	−0.6826	−0.4612
15	CoH_2	NPA	LANL2	−0.3817	−0.1316	0.4938	−0.6228	0.5296
16	RhH_2	Mulliken	LANL2	−0.5980	0.5480	0.0008	−0.2673	−0.0619
17	RhH_2	APT	LANL2	−0.2345	0.0055	0.7713	−0.6902	−0.3183
18	RhH_2	NPA	LANL2	−0.3756	−0.1323	0.5004	−0.6128	0.4189
19	IrH_2	Mulliken	LANL2	−0.7603	0.6146	0.0288	−0.2689	−0.1720
20	IrH_2	APT	LANL2	−0.2216	0.0031	0.7953	−0.6883	−0.5133
21	IrH_2	NPA	LANL2	−0.3723	−0.1237	0.5238	−0.6035	0.5075
22	RuH_2	Mulliken	LANL2	−0.6083	0.5501	0.0068	−0.2766	−0.0867
23	RuH_2	APT	LANL2	−0.2324	0.0040	0.7689	−0.7052	−0.4038
24	RuH_2	NPA	LANL2	−0.4083	−0.1209	0.5000	−0.6420	0.1286
17	$RhMe_{cis}$	NPA	LANL2	−0.1311	−0.1499	0.5018	−0.6211	0.4137
18	$RhMe_{trans}$	NPA	LANL2	−0.1384	−0.1529	0.5129	−0.6198	0.4171
19	$IrMe_{cis}$	NPA	LANL2	−0.1302	−0.1418	0.5220	−0.6304	0.5033
20	$IrMe_{trans}$	NPA	LANL2	−0.1375	−0.1455	0.5345	−0.6122	0.5060
21	$RhPh_2$	NPA	LANL2	−0.0181	−0.1082	0.4950	−0.6066	0.4170
22	*o*-QM	NPA	6-311++G	−0.2058	−0.1661	0.4939	−0.5661[b]	–

[a] Effective core potentials are combined with D95** and 6-311++G is augmented with (3df,3pd) polarization functions. [b] CHelpG analysis of the B3LYP/6-311++G(d,p) structure resulted in partial charge of −0.56 for the *o*-QM oxygen atom.[24]

Table 3. Comparison of Factors Indicative of the Stability and Reactivity Reversal in *o*-QM Metal Complexes[a]

entry	cmpd	"hinge"	C^2-C^7	C^3-C^4	C^4-C^5	C^5-C^6	M-||[b]	M-||[c]	dihedral[d]	ν_{CO} (cm^{-1})	HOMO[e]	LUMO[e]	q on C^7
1	$IrMe_2$	37.7	1.366	1.460	1.437	1.461	2.053	2.051	7.6	1631	−0.183510	−0.038815	0.0913
2	$RhMe_2$	29.6	1.368	1.438	1.434	1.440	2.083	2.093	9.1	1613	−0.176050	−0.052419	0.0917
3	CoH_2	25.3	1.356	1.430	1.431	1.436	1.875	1.959	6.1	1617	−0.187387	−0.062233	−0.3817
4	RhH_2	26.9	1.355	1.435	1.436	1.440	2.099	2.111	6.0	1611	−0.182461	−0.059273	−0.3756
5	IrH_2	35.6	1.351	1.458	1.438	1.460	2.053	2.054	5.1	1632	−0.189966	−0.046043	−0.3723
6	RuH_2	25.2	1.356	1.439	1.433	1.442	2.101	2.108	9.1	1615	−0.178354	−0.037419	−0.4083
7	$RhMe_{cis}$	28.2	1.362	1.434	1.435	1.440	2.093	2.107	7.0	1618	−0.177787	−0.055685	−0.1311
8	$RhMe_{trans}$	28.4	1.358	1.437	1.436	1.440	2.095	2.108	6.1	1616	−0.178368	−0.054687	−0.1384
9	$IrMe_{cis}$	36.6	1.358	1.459	1.438	1.461	2.047	2.053	5.8	1642	−0.185600	−0.042635	−0.1302
10	$IrMe_{trans}$	36.8	1.354	1.460	1.438	1.461	2.048	2.049	5.3	1645	−0.186090	−0.040201	−0.1375
11	$RhPh_2$	28.2	1.376	1.436	1.434	1.437	2.097	2.112	16.1	1612	−0.175766	−0.062883	−0.0181
12	*o*-QM	–	1.342	1.346	1.448	1.348	–	–	0	1596	−0.239648	−0.108338	−0.2058

[a] Bond lengths are in Å and angles are in degrees. [b] Distance between metal atom and center of $C^3{=}C^4$ bond. [c] Distance between metal atom and center of $C^5{=}C^6$ bond. [d] Dihedral angle around carbonyl-methide portion of *o*-QM ligand, $\angle C^7{=}C^2{-}C^1{=}O$. [e] Energy levels are in hartrees.

$C^2{=}C^7$ bond by 0.02 Å, relative to the same bond in **RhH**$_2$, and the 2.9° larger $C^1{-}C^2{=}C^7$ angle confirms the steric effects of the phenyl group nearest the carbonyl function. Additional evidence of distortion is the lengthening of the *o*-QM−Rh distances for the outer carbons of the diene subunit by 0.01 and 0.03 Å for C^6 and C^3, respectively. The steric effects are best generalized by examining the twist in the exocyclic alkene unit relative to the *o*-QM ring, measured by the $O{=}C^1{-}C^2{=}C^7$ dihedral angle, which is 16.1° in **RhPh**$_2$, 9.1° in **RhMe**$_2$, 6.1 in **RhMe**$_{trans}$, 6.0° in **RhH**$_2$, and 5.8° in **RhMe**$_{cis}$.

The hinge angle is also only slightly affected by substitution and appears to increase by 1° for each methyl group on the exocyclic methylene carbon. However, the hinge angle of **RhPh**$_2$, 28.2°, is closer to that found in **RhH**$_2$ than in **RhMe**$_2$, **RhMe**$_{cis}$, or **RhMe**$_{trans}$. Electron-withdrawing substituents should stabilize the LUMO of the *o*-QM ligand and increase π back-donation. However, the finding may be rationalized in steric terms, wherein π back-bonding is reduced by the longer *o*-QM−Rh bonds. In either case the effect is minimal, as evidenced by only a 2.0° smaller hinge angle in **RhPh**$_2$ than in **RhMe**$_2$, but is indicative of stereoelectronic tuning of this angle and *o*-QM stability (Figure 15).

Population Analyses on the Optimized Geometries of *o*-QM Metal Complexes and the Parent *o*-QM. The partial charges derived from Mulliken, atomic polarizability tensor, and natural orbital analyses are presented in Table 2. Excluding the highly basis set-dependent metal atom, the Mulliken population analysis (std dev = 0.0071) displayed the most basis set dependence, followed by the APT (std dev = 0.0022) and then the NBO (std dev = 0.0001) analyses, both of which

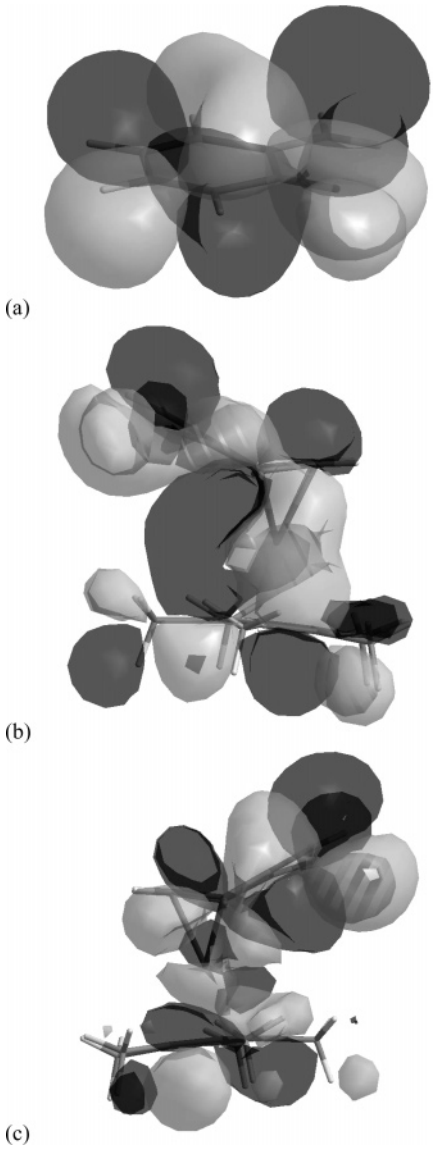

Figure 15. (a) LUMO of simple *o*-QM. (b) HOMO of $\mathbf{IrH}_2$. (c) LUMO of $\mathbf{IrH}_2$.

display very slight basis set variations. However, even the simple Mulliken analysis predicts the reactivity seen experimentally. Partial charges on C^7 of the unsubstituted complexes range from −0.5860 to −0.6083, whereas the unreactive disubstituted complexes $\mathbf{IrMe}_2$ and $\mathbf{RhMe}_2$ show slight positive charges at C^7. The APT charge distributions are considerably different than the Mullikens and also predict the trend seen in the reactivity. Negative charge buildup on C_{exo} in $\mathbf{MH}_2$ complexes is smaller, ranging from −0.2220 to −0.2345, and more positive charge is seen on C^7 of $\mathbf{MMe}_2$, 0.2323 and 0.2266. In the natural population analysis the nucleophilic C^7 of the $\mathbf{MH}_2$ complexes are negatively charged over the range of −0.3723 to −0.3817. Analogous to the other two population analyses, NPA predicts that the dimethyl-substituted congeners $\mathbf{MMe}_2$ will not be nucleophilic; both show slight positive charges of 0.0913 and 0.0917.

Monosubstitution of the *o*-QM ligand with a methyl group results in a partial negative charge on C^7 of −0.1311 to −0.1385. For comparative purposes, this is less negatively charged than C^7 of the simple *o*-QM, which has a charge of −0.2058. The trans isomer is about 0.007 more negatively charged than the cis isomer, which can be attributed to the inductive electronic effect of a zero degree dihedral between the electropositive carbonyl carbon, C^1, and the vinyl methyl carbon in the trans isomer. This is evident from the compensatingly smaller negative charge on the oxygen atom of the trans isomer relative to the cis isomer. The partial charges on the oxygen atom are −0.6211 and −0.6198 for $\mathbf{RhMe}_{cis}$ and $\mathbf{RhMe}_{cis}$, respectively, and −0.6304 and −0.6122 for $\mathbf{IrMe}_{cis}$ and $\mathbf{IrMe}_{cis}$, respectively. In the diphenyl-substituted rhodium complex, $\mathbf{RhPh}_2$, the charge on C^7 is slightly negative, −0.0181, as opposed to the dimethyl-substituted compound, $\mathbf{RhMe}_2$, which is slightly positively charge, 0.0913.

Conclusions

The stabilization and surprising reactivity reversal in the group 9 metal complexes of *o*-QM ligands has been explained by density functional theory calculations. We have applied these methods to gain insight into known *o*-QM metal complexes and predict the properties of additional complexes. The calculations accurately reproduce the geometry of these compounds found by X-ray diffraction. The stability is rationalized in terms of the hinge angle and the degree of $d-\pi^*$ back-bonding. The nucleophilic character of the exocyclic methide carbon is also correlated to these properties and is demonstrated by population analysis. The amount of negative charge on C^7 is affected by both the metal and the substituents. The partial charge and "hinge" angle follow the order Ru < Co < Rh < Ir. The Ru and Co complexes may be useful in future synthetic studies, because of their predicted high reactivity. We have also shown that monosubstitution may yield isolable nucleophilic metal complexes, which could prove important to the application of this chemistry to stereoselective synthesis.

Acknowledgment. This work was supported by a NSF-CNRS joint research project that H.A. and D.B.G. acknowledge. H.A. also thanks UPMC for supporting this work, and D.B.G. and D.A.L. acknowledge the partial support of SDSU in the form of travel money. The computations were performed on the SDSU Computational Science Program Intel Cluster, which is supported by a grant from the NSF (CHE-0216563).

Supporting Information Available: Electronic energies, Cartesian coordinates, and population analyses for computed structures referred to in the figures, tables, and Discussion. This material is available free of charge via the Internet at http://pubs.acs.org.

OM0504093